Engineering Analysis with Boundary Elements 35 (2011) 1256–1264

Contents lists available at ScienceDirect

Engineering Analysis with Boundary Elements

journal homepage: www.elsevier.com/locate/enganabound

Simulation of 3D flow in porous media by boundary element method

J. Kramer [a,*], J. Ravnik [b], R. Jecl [a], L. Škerget [b]

[a] Faculty of Civil Engineering, University of Maribor, Smetanova 17, SI-2000 Maribor, Slovenia
[b] Faculty of Mechanical Engineering, University of Maribor, Smetanova 17, SI-2000 Maribor, Slovenia

ARTICLE INFO

Article history:
Received 16 September 2010
Accepted 7 June 2011

Keywords:
Porous media
Boundary element method
Three-dimensional natural convection
Velocity–vorticity formulation
Brinkman-extended Darcy formulation

ABSTRACT

In the present paper problem of natural convection in a cubic porous cavity is studied numerically, using an algorithm based on a combination of single domain and subdomain boundary element method (BEM). The modified Navier–Stokes equations (Brinkman-extended Darcy formulation with inertial term included) were adopted to model fluid flow in porous media, coupled with the energy equation using the Boussinesq approximation. The governing equations are transformed by the velocity–vorticity variables formulation which separates the computation scheme into kinematic and kinetic parts. The kinematics equation, vorticity transport equation and energy equation are solved by the subdomain BEM, while the boundary vorticity values, needed as a boundary conditions for the vorticity transport equation, are calculated by single domain BEM solution of the kinematics equation. Computations are performed for steady state cases, for a range of Darcy numbers from 10^{-6} to 10^{-1}, and porous Rayleigh numbers ranging from 50 to 1000. The heat flux through the cavity and the flow fields are analyzed for different cases of governing parameters and compared to the results in some published studies.

© 2011 Elsevier Ltd. All rights reserved.

1. Introduction

Buoyancy induced flows in saturated porous media have been the subject of intense research over the last few decades, mainly because of several important industrial and environmental applications, e.g. building thermal insulation, geothermal systems, petroleum reservoirs, etc. Several studies have been published focusing on the problem of natural convection in porous enclosures, mainly for the cases of two-dimensional geometries where temperature gradient is imposed either horizontally [1–6] or vertically [7–10]. Less attention has been dedicated to three-dimensional configurations, which are rare and primarily confined to conditions of heating from below and using the Darcy model. Only few studies can be found considering a 3D enclosure heated from the side. One of them is a study of Dawood and Burns [11], where they reported that heat flow under these conditions depends on a Rayleigh number, geometry and boundary conditions, and that the flow patterns are much more complicated in three than in two dimensions. Sharma and Sharma [12] investigated the non-Darcy effects of 3D natural convection in a porous box, focusing on the influence of the Brinkman viscous and Forchheimer non-linear inertial terms and concluded, these effects are significant at high Rayleigh numbers and low values of Darcy and Forchheimer numbers. Recently, Wang et al. [13] published a 3D study of natural convection in an inclined porous enclosure under magnetic field, using the Brinkman–Forchheimer extended Darcy model. They investigated an influence of an inclination angle, magnetic force and Darcy number. They reported that heat transfer is enhanced with the increase in the inclination angle and the Darcy number. The implied magnetic force, which is acting against the gravitational force has also big influence on the averaged Nusselt number values. Wang et al. [14] investigated 3D natural convection in an inclined porous cavity with time oscillating boundary conditions. They found out that in case of moderate inclined cavity, convective flow inside a cavity is stable, regular and mainly 2D. In cases of higher inclination angles, flow patterns become unstable and complicated, 3D multiple roll cells are established.

There exist several comprehensive studies of a problem of 3D natural convection in porous cavities heated from below. At the beginning the problem was studied mostly analytically with the aim to determine critical values of Rayleigh numbers, when the flow in this configuration becomes unstable (convective). The studies based on the linear theory or energy method for convective instability such as reported in paper of Beck [15]. Holst and Aziz [16] published a numerical study of transient 3D natural convection in porous media and reported that under certain conditions 3D motion would result in significantly higher heat transfer rates than 2D motion at the same Rayleigh number. Zebib and Kassoy [17]

* Corresponding author.
E-mail addresses: janja.kramer@uni-mb.si (J. Kramer), jure.ravnik@uni-mb.si (J. Ravnik), renata.jecl@uni-mb.si (R. Jecl), leo@uni-mb.si (L. Škerget).

0955-7997/$ - see front matter © 2011 Elsevier Ltd. All rights reserved.
doi:10.1016/j.enganabound.2011.06.002

published analytical study, where they obtained critical Rayleigh numbers for the onset of convection, where large temperature differences are applied, including the viscosity variation with temperature. They reported that the critical Rayleigh number is reduced from the value, which is predicted by constant viscosity calculations. In the second study [18] they derived expressions for 2D and 3D Nusselt numbers and stated that in case of 2D, heat is transferred more efficiently than in 3D cases, when the Rayleigh number is just above the critical value. The same results for Nusselt numbers at low values of the Rayleigh number were published by Straus and Schubert [19], where the results are obtained using a numerical methods. Schubert and Straus [20] investigated multicellular steady and unsteady convection for 2D and 3D cases with the use of the Galerkin approach. They investigated different situations where convective flow becomes unsteady and reported in which case more heat is transferred. Horne [21] published numerical results that demonstrate that there exists more than one mode of convection for any particular physical configuration and Rayleigh number. Kimura et al. [22] investigated time dependent convection using a pseudospectral based numerical scheme. They obtained the evolution of convective regimes with increasing *Ra* from symmetric steady state to oscillatory flow and stated that the critical Rayleigh number for the onset of oscillation is higher for 3D case and the Nusselt number of 3D flows is generally greater than that of the 2D flows. Stamps et al. [23] studied natural convection in a cube of fluid-saturated porous medium heated from below at insulated vertical sides and the special case where heat is transferred through the vertical sides. They identified three distinct flow patterns depending on the rate of heat transfer and the Rayleigh number. Recently, Neto et al. published studies considering transient 3D natural convection in cubic porous cavity [24], and cavities with different aspect ratios [25] using the integral transform method employing the vorticity-vector potential formulation. Sezai [26] studied flow patterns in a fluid-saturated porous cube heated from below using a non-Darcy flow model. He reported about some new flow patterns in addition to the already published studies.

In this paper a numerical method for the simulation of fluid flow and heat transfer in porous media for steady flow cases, based on the boundary element method solution of the Navier–Stokes equations in velocity–vorticity form is presented. The proposed algorithm is based on the pure fluid [27] and nanofluid [28] simulation codes. The algorithm accepts Dirichlet or Neumann type boundary conditions for velocity and temperature, while it calculates boundary values of vorticity using single domain BEM. The vorticity and energy transport equations are solved using a domain decomposition BEM approach [29].

2. Mathematical formulation

2.1. Governing equations

Transport phenomena in porous media can be described with macroscopic Navier–Stokes equations, which are obtained by averaging of the general microscopic equations, written for the pure fluid flow, over sufficiently large representative elementary volume (REV). Only one part of the volume, which is expressed with the porosity ϕ, is available for the fluid flow [30]. The REV has to be determined in a way that, irrespective of its position in porous media, it always contains both solid and fluid phases. In the model development following assumptions are adopted: the fluid flow is steady and laminar, the solid phase is homogeneous, isotropic and non-deformable, the fluid is incompressible Newtonian and in thermal equilibrium with the solid phase. The porosity and permeability of porous medium are constant, while the density of the fluid depends only on temperature variations and is described with the Oberbeck Boussinesq approximation as

$$\rho = \rho_0(1-\beta_T(T-T_0)). \tag{1}$$

In the above expression ρ is the density of the fluid, T is the temperature and β_T is the volumetric thermal expansion coefficient given with $\beta_T = -1/\rho[\partial\rho/\partial T]$. The subscript 0 refers to a reference state.

The macroscopic conservation equations can now be written as:

- Continuity equation

$$\vec{\nabla}\cdot\vec{v} = 0. \tag{2}$$

- Momentum equation

$$\frac{1}{\phi}\frac{\partial\vec{v}}{\partial t} + \frac{1}{\phi^2}(\vec{v}\cdot\vec{\nabla})\vec{v} = -\beta_T(T-T_0)\vec{g} - \frac{1}{\rho_0}\vec{\nabla}p + \frac{1}{\phi}\nu\nabla^2\vec{v} - \frac{\nu}{K}\vec{v}. \tag{3}$$

- Energy equation

$$\sigma\frac{\partial T}{\partial t} + (\vec{v}\cdot\vec{\nabla})T = \frac{\lambda_e}{c_f}\nabla^2 T. \tag{4}$$

The parameters used above are: $\vec{v}$, volume averaged velocity, ϕ, porosity, t, time, ρ, density, ν, kinematic viscosity, p, pressure, $\vec{g}$, gravity vector, K, permeability. In the energy equation σ represents the heat capacity ratio $\sigma = (\phi c_f + (1-\phi)c_s)/c_f$, where $c_f = (\rho c_p)_f$ and $c_s = (\rho c_p)_s$ are heat capacities for fluid and solid phases, respectively. λ_e is the effective thermal conductivity of the fluid saturated porous media given as $\lambda_e = \phi\lambda_f + (1-\phi)\lambda_s$, where λ_f and λ_s are thermal conductivities for fluid and solid phases, respectively.

The momentum equation (3) is also known as the Darcy–Brinkman equation, with two viscous terms, e.g. Brinkman viscous term (third on the r.h.s.) and Darcy viscous term (fourth on the r.h.s.).

The Brinkman viscous term is originally given as $\nu_{eff}\nabla^2\vec{v}$, where ν_{eff} is the effective viscosity. Brinkman set ν and ν_{eff} equals to each other but in general, that is not true [31]. The viscosity ratio can be introduced as $\Lambda = \nu_{eff}/\nu$. For an isotropic porous medium the averaging process leads to the result that $\Lambda = 1/\phi T^*$, where T^* is the tortuosity of the medium [32]. Since Λ depends on the geometry of the medium, its value is often approximated by $\Lambda = 1/\phi$, in cases with a high value of porosity, a reasonable approximation is to be $\Lambda = 1$ [32,4]. In the present study, the viscosity ratio is assumed to be $\Lambda = 1/\phi$, which results in a Brinkman term, e.g. $1/\phi\nu\nabla^2\vec{v}$.

The Brinkman viscous term is analogous to the Laplacian term in the classical Navier–Stokes equations for pure fluid flow. It expresses the viscous resistance or viscous drag force exerted by the solid phase on the flowing fluid at their contact surfaces. With the Brinkam term the non-slip boundary condition on a surface which bounds porous media is satisfied [31].

2.2. Velocity–vorticity formulation

The velocity–vorticity formulation of above given modified Navier–Stokes equations is derived by taking the curl of the mass conservation law (2), and of the Brinkman momentum equation (3). The vorticity is defined as the curl of the velocity field $\vec{\omega} = \vec{\nabla}\times\vec{v}$ and is solenoidal by the definition, $\vec{\nabla}\cdot\vec{\omega} = 0$. As a consequence of the transformation, the computational scheme is partitioned into its kinematic and kinetic parts [33]. The kinematics is given with the elliptic velocity vector equation:

$$\nabla^2\vec{v} + \vec{\nabla}\times\vec{\omega} = 0, \tag{5}$$

furthermore, the kinetic part is governed by the vorticity transport equation:

$$\phi\frac{\partial\vec{\omega}}{\partial t}+(\vec{v}\cdot\vec{\nabla})\vec{\omega}=(\vec{\omega}\cdot\vec{\nabla})\vec{v}-\vec{\nabla}\times(\beta_T\phi^2(T-T_0)\vec{g})+\nu\phi\nabla^2\vec{\omega}-\frac{\nu\phi^2}{K}\vec{\omega}. \tag{6}$$

2.3. Non-dimensional equations

Before all equations will be rewritten in the non-dimensional form, in the vorticity and energy equations the modified vorticity and temperature time steps are introduced as $t_\omega=t/\phi$ and $t_T=t/\sigma$. These are necessary mathematical steps allowing to use the numerical scheme presented in the following section. The vorticity and energy equations are now given as

$$\frac{\partial\vec{\omega}}{\partial t_\omega}+(\vec{v}\cdot\vec{\nabla})\vec{\omega}=(\vec{\omega}\cdot\vec{\nabla})\vec{v}-\vec{\nabla}(\beta_T\phi^2(T-T_0)\vec{g})+\nu\phi\nabla^2\vec{\omega}-\frac{\nu\phi^2}{K}\vec{\omega}, \tag{7}$$

$$\frac{\partial T}{\partial t_T}+(\vec{v}\cdot\vec{\nabla})T=\frac{\lambda_e}{c_f}\nabla^2 T. \tag{8}$$

The non-dimensional form is obtained using following dimensionless variables:

$$\vec{v}\to\frac{\vec{v}}{v_0},\quad \vec{r}\to\frac{\vec{r}}{L},\quad \vec{\omega}\to\frac{\vec{\omega}L}{v_0},\quad t_\omega\to\frac{v_0 t_\omega}{L},$$

$$t_T\to\frac{v_0 t_T}{L},\quad T\to\frac{T-T_0}{\Delta T},\quad \vec{g}\to\frac{\vec{g}}{g_0}, \tag{9}$$

where v_0, L and T_0 are the characteristic velocity, length and temperature, respectively. Furthermore, ΔT is the characteristic temperature difference and g_0 the gravity acceleration $g_0=9.81\ \mathrm{m/s^2}$. Characteristic velocity is given with the expression $v_0=\lambda_f/(c_f L)$, which is a common choice for buoyant flow simulations. In addition, the pure fluid Rayleigh (Ra_f), Prandtl (Pr), Darcy (Da) and porous Rayleigh (Ra_p) numbers are defined as

$$Ra_f=\frac{g_0\beta_T\Delta T L^3}{\nu\alpha}, \tag{10}$$

$$Pr=\frac{\nu}{\alpha}, \tag{11}$$

$$Da=\frac{K}{L^2}, \tag{12}$$

$$Ra_p=Ra_f\,Da=\frac{g_0\beta_T\Delta T L K}{\nu\alpha}, \tag{13}$$

where α is the thermal diffusivity and is given with $\alpha=\lambda_f/c_f$. The non-dimensional vorticity and energy equations for the simulation of fluid flow in porous media can now be written as

$$\frac{\partial\vec{\omega}}{\partial t_P}+(\vec{v}\cdot\vec{\nabla})\vec{\omega}=(\vec{\omega}\cdot\vec{\nabla})\vec{v}+Pr\,\phi\nabla^2\vec{\omega}-Pr\,Ra_f\phi^2\vec{\nabla}T\vec{g}-\frac{Pr}{Da}\phi^2\vec{\omega}, \tag{14}$$

$$\frac{\partial T}{\partial t_T}+(\vec{v}\cdot\vec{\nabla})T=\frac{\lambda_e}{\lambda_f}\nabla^2 T. \tag{15}$$

The flow and heat transfer in porous medium are thus defined by specifying the fluid Rayleigh, Prandtl and Darcy number values.

3. Numerical method

3.1. Integral form of governing equations

Considering a domain Ω with a boundary Γ, a fundamental solution of the Laplace equation and the Gauss and Greens theorems are used to write the integral kinematics equation without derivatives of the velocity or vorticity fields [34]:

$$c(\xi)\vec{v}(\xi)+\int_\Gamma\vec{v}(\vec{n}\cdot\vec{\nabla})u^\star\,d\Gamma=\int_\Gamma\vec{v}\times(\vec{n}\times\vec{\nabla})u^\star\,d\Gamma+\int_\Omega(\vec{\omega}\times\vec{\nabla}u^\star)\,d\Omega. \tag{16}$$

Here $\vec{\xi}$ is the source or collocation point, $\vec{n}$ is a vector normal to the boundary, pointing out of the domain and $u^\star$ is the fundamental solution: $u^\star=1/4\pi|\vec{\xi}-\vec{r}|$. In order to have a non-singular system of equations for solving for boundary values of vorticity, a tangential form of Eq. (16) is used. It is obtained by a cross product with a unit normal, yielding

$$c(\vec{\xi})\vec{n}(\vec{\xi})\times\vec{v}(\vec{\xi})+\vec{n}(\vec{\xi})\times\int_\Gamma\vec{v}\vec{\nabla}u^\star\cdot\vec{n}\,d\Gamma=\vec{n}(\vec{\xi})\times\int_\Gamma\vec{v}\times(\vec{n}\times\vec{\nabla})u^\star\,d\Gamma+\vec{n}(\vec{\xi})\times\int_\Omega(\vec{\omega}\times\vec{\nabla}u^\star)\,d\Omega. \tag{17}$$

The same fundamental solution and a standard BEM derivation [35] are used to write the integral forms of the vorticity transport equation (14) and of the energy equation (15):

$$\begin{aligned}c(\vec{\xi})\omega_j(\vec{\xi})+&\int_\Gamma\omega_j\vec{\nabla}u^*\cdot\vec{n}\,d\Gamma\\&=\int_\Gamma u^* q_j\,d\Gamma+\frac{1}{Pr}\frac{1}{\phi}\left(\int_\Gamma\vec{n}\cdot\{u^*(\vec{v}\omega_j-\vec{\omega}v_j)\}\,d\Gamma-\int_\Omega(\vec{v}\omega_j-\vec{\omega}v_j)\cdot\vec{\nabla}u^*\,d\Omega\right)\\&\quad-Ra_f\phi\int_\Gamma(u^*T\vec{g}\times\vec{n})_j\,d\Gamma-Ra_f\phi\int_\Omega(T\vec{\nabla}\times u^*\vec{g})_j\,d\Omega\\&\quad+\frac{1}{Da}\phi\int_\Omega\omega_j u^*\,d\Omega,\end{aligned} \tag{18}$$

$$c(\vec{\xi})T(\vec{\xi})+\int_\Gamma T\vec{\nabla}u^*\cdot\vec{n}\,d\Gamma=\int_\Gamma u^* q_T\,d\Gamma+\frac{\lambda_f}{\lambda_e}\times\left(\int_\Gamma\vec{n}\cdot\{u^*(\vec{v}T)\}\,d\Gamma-\int_\Omega(\vec{v}T)\cdot\vec{\nabla}u^*\,d\Omega\right). \tag{19}$$

Here ω_j is a vorticity component, q_j is a component of vorticity flux and q_T is the heat flux. In the present study, only steady flow fields will be considered, thus the time derivative terms $\partial\omega/\partial t_\omega$ and $\partial T/\partial t_T$ are omitted.

A combination of subdomain BEM and single domain BEM for the solution of the governing equations will be applied. The Dirichlet and/or Neumann boundary conditions for velocity and temperature are given. They are used to obtain solutions of the kinematics equation (16) for domain velocity values and energy equation (19) for domain temperature values. The boundary conditions for vorticity, which are needed to solve the vorticity transport equation (18), are unknown. The single domain BEM of the tangential form of the integral kinematics equation (17) will be used to obtain the unknown boundary vorticity values. The outline of the algorithm is as follows:

- Initialization, calculate integrals, set up parameters.
- Begin non-linear loop:
  - Calculate boundary vorticity values by solving the tangential form of the kinematics equation (17) by single domain BEM.
  - Calculate domain velocity values by solving the kinematics equation (16) by subdomain BEM.
  - Solve the energy equation (19) using the new velocity field for domain temperature values by subdomain BEM.
  - Solve vorticity transport equation (18) by subdomain BEM for domain vorticity values using the boundary values from the solution of the kinematics equation and new velocity and temperature fields.

- Check convergence — repeat steps in the non-linear loop until convergence of all field functions is achieved.
- End non-linear loop.
- Output results.

In the subdomain BEM method, which is used to solve Eqs. (16), (18) and (19) a mesh of the entire domain Ω is made, each mesh element is named as a subdomain. Equations are written for all source points on each of the subdomains. In order to obtain a discrete version of integral equations we use shape functions to interpolate field functions and flux across the boundary and inside the subdomain. In this work hexahedral subdomains with 27 nodes are used, which enable continuous quadratic interpolation of field functions. The boundary of each hexahedron consists of six boundary elements. On each boundary element the flux is interpolated using discontinuous linear interpolation scheme with four nodes. By using discontinuous interpolation, flux definition problems in corners and edges could be avoided. Between subdomains, the functions and their fluxes are assumed to be continuous. The resulting linear systems of equations are overdetermined and sparse. They are solved in a least-squares manner. Discretization procedure for the single domain BEM, which is used to solve Eq. (17), is analogous, with a distinction that source points are set into all nodes on the boundary of the entire domain. The resulting linear system of equations is full. It is solved by the LU decomposition method. This algorithm has been proposed for 3D fluid flow and heat transfer by Ravnik et al. [27]. In the present work, the algorithm for simulations in porous media was expanded. The kinematics equation requires no changes, while porous parameters had to be introduced in vorticity transport and energy equations. The Darcy term in the vorticity transport equation, which is not present in the pure fluid case, is linearly proportional to the unknown vorticity, thus it was included into the system matrix.

4. Test cases

The physical model, where the above presented numerical scheme was tested, is a 3D cube enclosure filled with fluid saturated porous medium. One vertical wall is isothermally heated, the opposite isothermally cooled, all other walls are adiabatic and impermeable as shown in Fig. 1. The boundary conditions for the test example can be written as:

- $v_x = v_y = v_z = 0$ for $x = y = z = 0$ and $x = y = z = L$;
- $T = 0.5$ for $x = 0$;
- $T = -0.5$ for $x = L$;
- $\partial T/\partial y = 0$ for $y = 0$ and $y = L$;
- $\partial T/\partial z = 0$ for $z = 0$ and $z = L$.

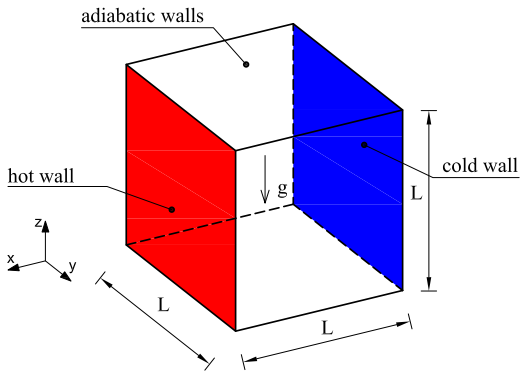

Fig. 1. Geometry of the problem.

Natural convection phenomena in fluid saturated porous medium are expected to depend on a number of parameters, such as porosity, thermal conductivity and heat capacity of fluid and solid phases, viscosity of the fluid phase, etc. The wall heat flux is calculated for different values of porous Rayleigh number ($Ra_P = 50$, 100, 200, 500 and 1000) and Darcy numbers ($10^{-6} \le Da \le 10^{-1}$), which can be expressed in terms of average Nusselt number given as

$$Nu = \int_{\Gamma} \vec{\nabla} T \cdot \vec{n}\, d\Gamma, \tag{20}$$

where Γ is the surface through which the heat flux is calculated and $\vec{n}$ is a unit normal to this surface.

The calculations were performed on a non-uniform mesh with $20 \times 8 \times 20$ subdomains and 28 577 nodes. Subdomains are concentrated towards the hot and a cold walls. The convergence criteria for all field functions were 10^{-5}, under-relaxation of vorticity and temperature values ranging from 0.1 to 0.01 were used.

In order to validate the numerical scheme for the 3D formulation, first a 2D simulation of flow of air ($Pr = 0.71$) in a differentially heated porous cavity was done. To perform a 2D simulation using a 3D code, a thin layer domain was created ($x = z = L$, $y = L/10$) and symmetry boundary conditions were applied on the $y = 0$ and $y = L/10$ walls. The used mesh had $20 \times 1 \times 20$ subdomains and in total 5043 nodes. The subdomains were concentrated towards the hot and cold walls. The results were compared to two published 2D studies of Jecl et al. [36] and Lauriat and Prasad [3], where the case of natural convection in a rectangular porous cavity is considered. In both studies the Brinkman-extended Darcy model with inertial term included is used. The comparison is shown in Table 1 and it can be observed that there is a good agreement between the results of the present study for the case of thin porous layer and published 2D studies.

Table 2 presents Nusselt number values for the cubic enclosure for $Pr = 0.71$, $\phi = 0.8$, $Ra_P = 1000$ and different values of Da. The results are compared to the study of authors Sharma and Sharma [12], where the 3D natural convection in a porous box is considered, and the fluid flow is modeled with the use of the Darcy–Brinkman–Forchheimer model. Very good agreement between the results can be observed for the case of high Darcy number values ($Da = 10^{-4}$–10^{-2}). Slight differences occur in case of very low Darcy numbers ($Da = 10^{-5}$ and 10^{-6}). In this case the effect of the Forchheimer term, which is not included in the model of the present study, becomes significant and influences the overall heat transfer resulting in lower values of Nusselt numbers [12].

In addition, Nusselt number values for natural convection for $Pr = 0.71$, $\phi = 0.8$, $Ra_P = 50$, 100, 200 and 500 and $10^{-6} \le Da \le 10^{-1}$ are presented in Table 3. The comparison of Nusselt number

Table 1
Nusselt number values for the 2D natural convection in a thin layer ($x = z = L$, $y = L/10$) heated from the side for $Ra_P = 100$ and 500, $\phi = 0.8$ and different values of Darcy number. The results are compared to the studies of Jecl et al. [36] and Lauriat and Prasad [3].

Ra_P/Da	10^{-1}	10^{-2}	10^{-3}	10^{-4}	10^{-5}	10^{-6}
100						
Present	1.063	1.632	2.369	2.875	3.165	3.256
[36]	1.088	1.695	2.414	2.847	2.995	–
[3]	–	1.70	2.41	2.84	3.02	3.09
500						
Present	1.593	3.058	5.160	7.259	8.699	9.122
[36]	1.681	3.145	5.235	7.185	8.428	–
[3]	–	3.30	5.42	7.35	8.41	8.84

values for different parameters is presented graphically in Fig. 2. From the graph it can be observed that the Nusselt number is increasing with the decrease in *Da* and increase in Ra_P. The influence of the Darcy number is more pronounced at higher values of porous Rayleigh number. At low values of Ra_P the Nusselt number values are near to 1, the dominant heat transfer mechanism in this case is conduction. This changes with increasing the Ra_P and decreasing of *Da*, when convection becomes dominant while conduction is negligible. When values of *Da* are high, the Brinkman viscous term in the momentum equation plays a significant role and reduces the overall heat transfer, which results in smaller values of *Nu*. With the decrease in *Da*, the influence of Brinkman viscous term becomes almost negligible ($Da < 10^{-4}$). In that case viscous effects become smaller and the inertial effect becomes significant due to high fluid velocity. For low values of the Darcy number the model gives similar results as the classical Darcy model [4].

Table 2
Nusselt number values for the 3D natural convection in a cube for $Ra_P=1000$, $\phi=0.8$ and different values of Darcy number. The results are compared to the study of Sharma and Sharma [12].

Ra_P/Da	10^{-1}	10^{-2}	10^{-3}	10^{-4}	10^{-5}	10^{-6}
1000						
Present	1.855	3.770	6.922	10.558	13.242	14.568
[12]	–	3.99	6.95	10.14	12.78	13.72

Table 3
Nusselt number values for the 3D natural convection in a cube for $Ra_P=50$, 100, 200 and 500, $\phi=0.8$ and different values of Darcy number.

Ra_P/Da	10^{-1}	10^{-2}	10^{-3}	10^{-4}	10^{-5}	10^{-6}
50	1.010	1.216	1.635	1.949	2.113	2.175
100	1.039	1.533	2.331	2.957	3.295	3.431
200	1.132	2.029	3.341	4.496	5.168	5.456
500	1.453	2.920	5.148	7.462	9.015	9.728

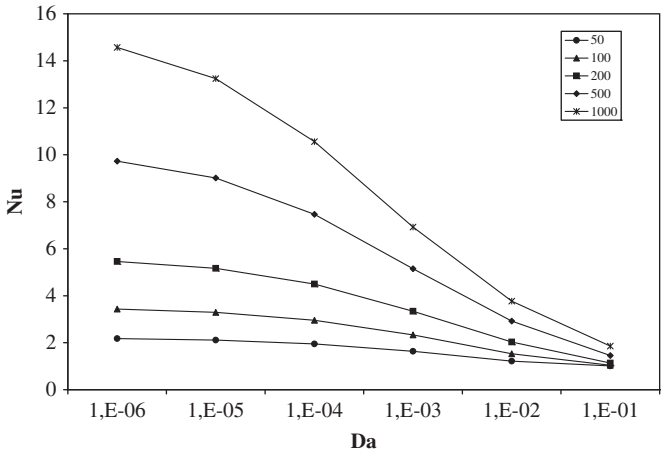

Fig. 2. Dependence of the Nusselt number on the Darcy number for different values of porous Rayleigh numbers.

Fig. 3 the temperature profiles for $Ra_p=100$, 500 and 1000 and different values of *Da* are presented. The temperature gradients increase with the decrease in *Da*. The highest temperature gradients can be observed close to the hot and cold walls in case of $Ra_P=1000$. When $Ra_P=100$ all profiles are close to the linear profile. In that case the Nusselt number is close to unity, and the heat is transferred mainly by conduction. Temperature contours on the plane $y=0.5$ for different values of Ra_P and *Da* are displayed in Fig. 4. The temperature field is observed to be stratified in all cases (layers of fluid with equal temperature are perpendicular to the direction of gravity), especially in the central part of the cube.

In the chosen geometry, the onset of natural convection induces the main vortex in the x–z plane, so the $y=0.5$ plane is chosen to study the velocity profiles. Vertical velocity profiles $v_z(x,0.5,0.5)$ and horizontal velocity profiles $v_x(0.5,0.5,z)$ across the center of the cube are shown in Fig. 5. Furthermore, the streamlines for different values of Ra_P and *Da* in the plane $y=0.5$ are shown in Fig. 6. The symmetry of the flow field in the plane $y=0.5$ can be observed, which indicates 2D flow behavior in that plane, where $v_y=0$. It can be clearly seen that the fluid is moving faster along the hot and cold walls, where streamlines are closely spaced. Higher values of velocity are also observed at the top and bottom walls. In the limit case, when $Da\to 0$ (Darcy law), the maximum velocity is on the boundaries. In that case the viscous effect described with the Brinkman term becomes almost negligible and the boundary effects are insignificant. With the increase in *Da* number the viscous effect becomes more important and slows down the fluid motion. The streamlines are observed to be more sparsely spaced near the solid boundaries and the region, where the flow has a maximum velocity is moved away from the solid walls towards the core region.

From the flow structure in the enclosure it can be examined that the flow field is not far from being 2D. This is due to the fact

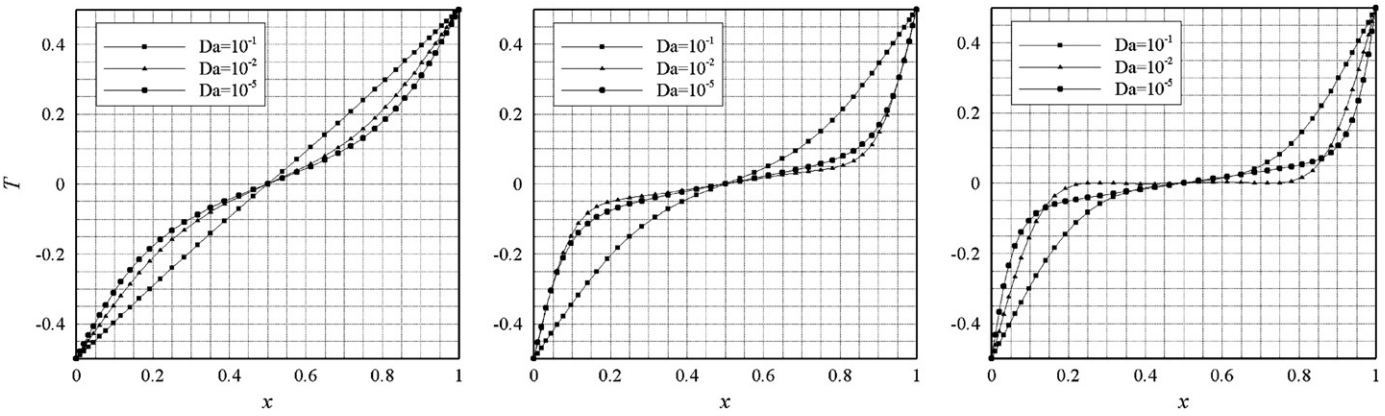

Fig. 3. Temperature profiles for $Ra_P=100$ (left), $Ra_P=500$ (middle) and 1000 (right) at $y=0.5$ and $z=0.5$.

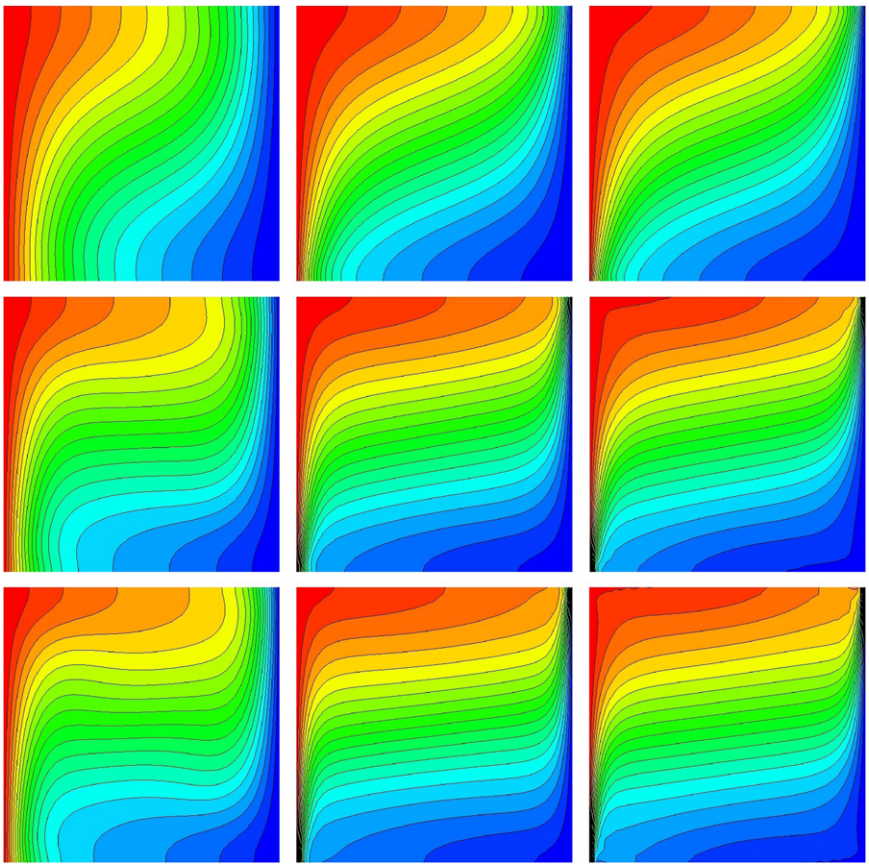

Fig. 4. Temperature contour plots on the $y=0.5$ plane for $Ra_P=100$ (above), 500 (middle) and 1000 (bottom) and the Darcy number $Da=10^{-2}$ (left), 10^{-4} (middle) and 10^{-6} (right).

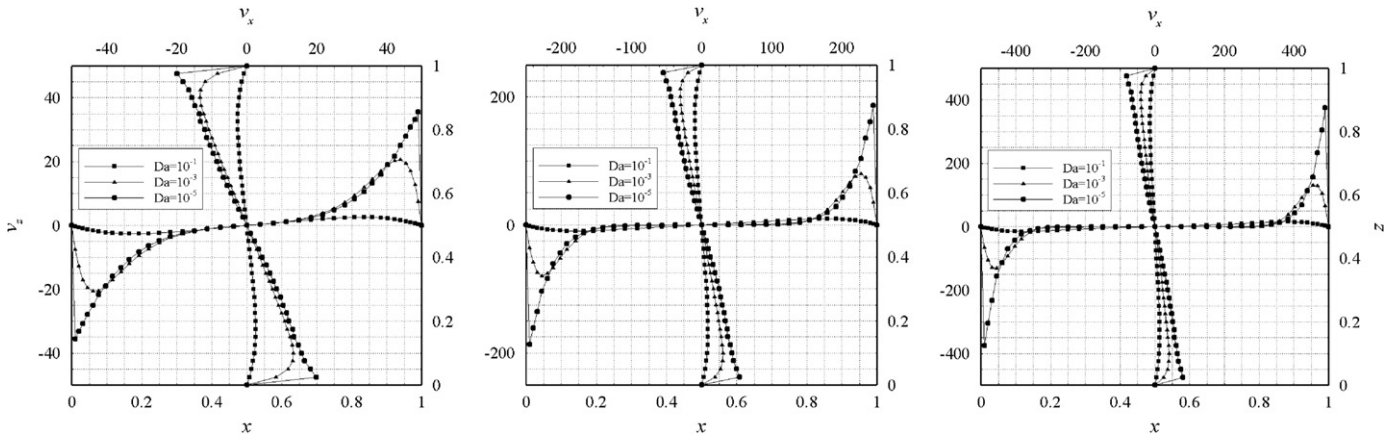

Fig. 5. Velocity profiles $v_x(0.5,0.5,z)$ and $v_z(x,0.5,0.5)$ for $Ra_P=100$ (left), 500 (middle) and 1000 (right) at $y=0.5$ and $z=0.5$.

that the flow field is driven by a temperature difference between two opposite walls, which causes large 2D vortex in the y plane. The 3D nature of the phenomena can be observed in the corners of the domain, which can be clearly seen from the iso-surfaces of absolute value of y velocity component plotted in Fig. 7. The extent of movement perpendicular to the plane of the main vortex is small, but it becomes more apparent in case of higher Ra_p and lower values of Da.

In Fig. 8 temperature profiles along the y axis are shown for different locations in the cube. It can be observed that in the center of the cube temperature is constant and it does not change in the y direction. From the profiles in the corners of the cube some fluctuations of the temperature in the y direction can be observed, which is a result of 3D motion.

Finally in Fig. 9 the y vorticity component contours along the walls of the enclosure are shown. The vorticity values grow rapidly, especially with the decrease in Da as well as with the increase in Ra_P. This is again due to the influence of viscous term, which is negligible in case of small values of Da, so higher velocity gradients are produced along the solid walls. The highest values are found at the bottom of the hot and at the top of the cold wall, where also the highest velocity gradients occur.

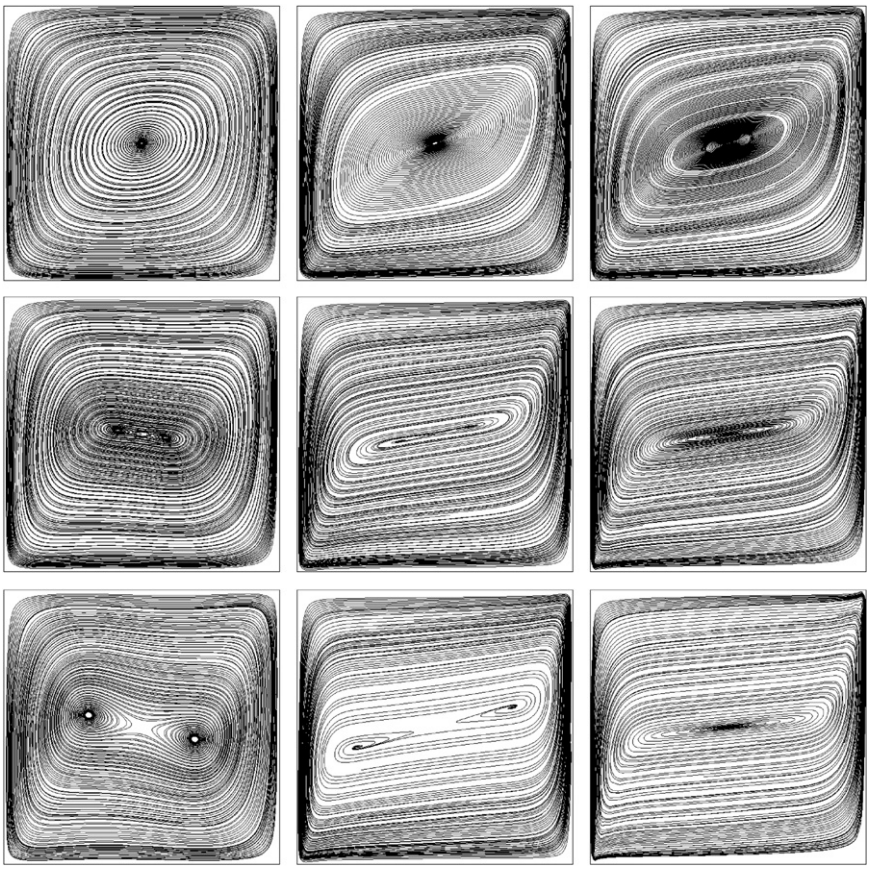

Fig. 6. Streamlines on the $y=0.5$ plane for $Ra_P=100$ (above), 500 (middle) and 1000 (bottom) and the Darcy number $Da=10^{-2}$ (left), 10^{-4} (middle) and 10^{-6} (right).

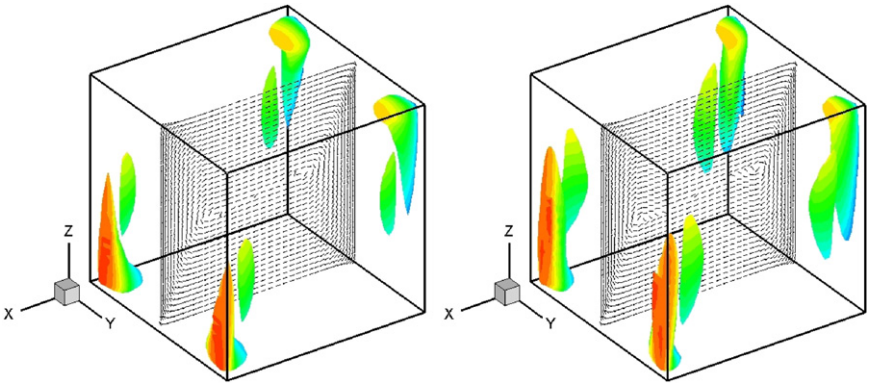

Fig. 7. Iso-surfaces for $Ra_P=500$, $Da=10^{-3}$ and absolute value of velocity component $|v_y|=3$ (left) and $Ra_P=1000$, $Da=10^{-3}$, $|v_y|=7$ (right). Contours of temperature are displayed on the iso-surfaces ($-0.5<T<-0.5$). In addition, the velocity vectors on the plane $y=0.5$ are displayed.

5. Summary

3D natural convection in a cube enclosure filled with porous media was investigated numerically using the boundary element method. The Brinkman extended Darcy formulation with inertial term included was used to model fluid flow in porous media. The velocity–vorticity formulation of governing equations was obtained. A single domain BEM solution of the kinematics equation was used to obtain the boundary vorticity values. The vorticity equation for the domain vorticity values, energy equation for the domain temperature values and kinematics equation for the domain velocity values were solved by the use of subdomain BEM.

The results of overall heat transfer through the enclosure are given in terms of Nusselt number values and compared to some published studies. It may be observed that the effect of Brinkman viscous term becomes significant when $Da>10^{-4}$ and is more pronounced at higher values of porous Rayleigh number. The results show that the Darcy number values strongly affect both heat transfer rate as well as the flow regime. With the decrease in the Da the temperature gradients near the solid boundaries increase, the same can be observed for the velocity gradients. The heat transfer through enclosure is enhanced with the decrease in Da and increase of Ra_P. The temperature field in the enclosure shows typical stratified structure where the layers of constant temperature are perpendicular to the gravity direction.

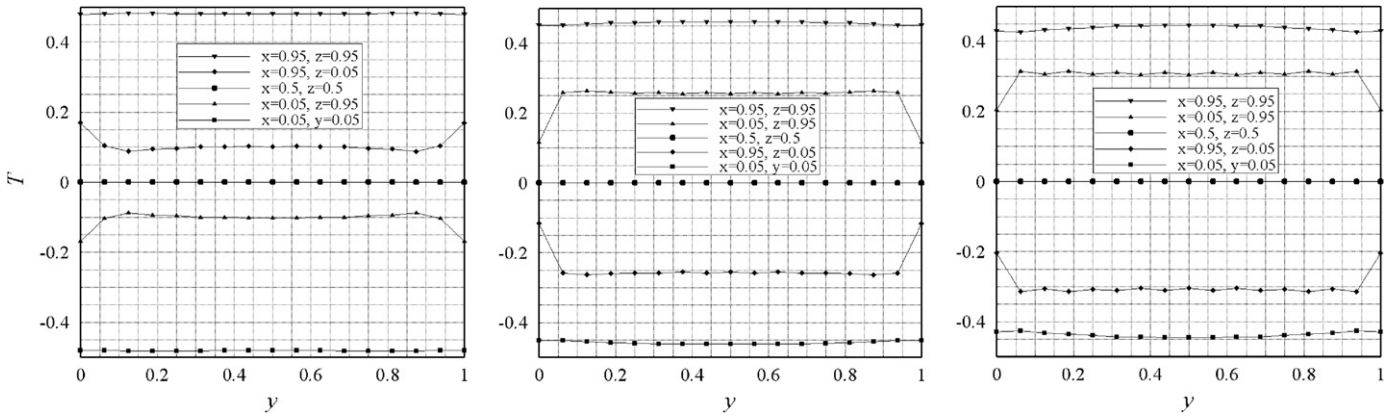

Fig. 8. Temperature profiles along y axis for $Ra_P=100$ (left), 500 (middle) and 1000 (right), $Da=10^{-5}$ at different locations in the cube.

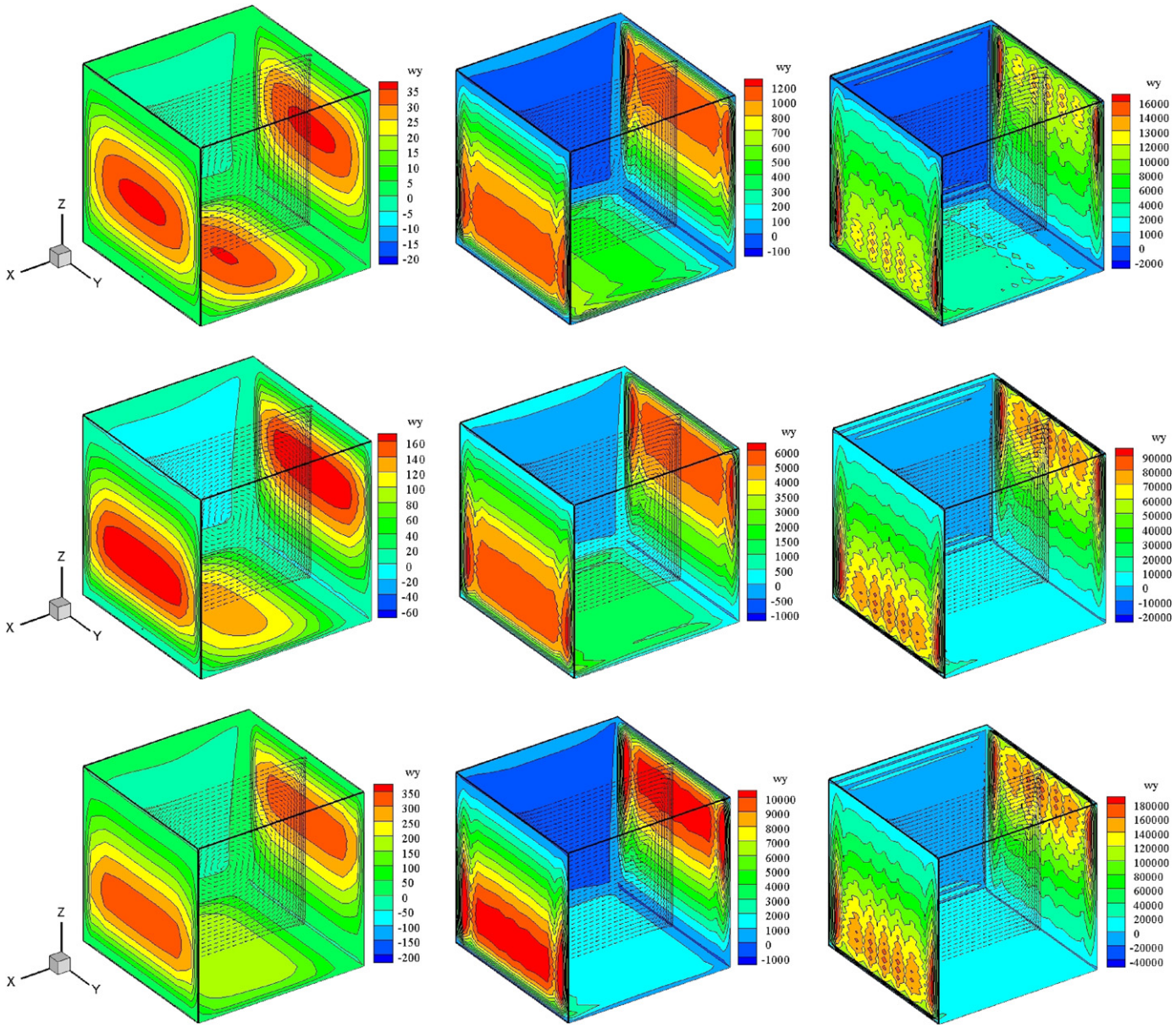

Fig. 9. Contours of the y component of vorticity, ω_y, for $Ra_P=100$ (above), 500 (middle) and 1000 (bottom) and $Da=10^{-1}$ (left), 10^{-3} (middle) and 10^{-5} (right). In addition the velocity vectors are illustrated on the plane $y=0.5$.

Thee-dimensional nature of the flow field was observed in the corners of the enclosure, although the fluid is moving predominantly in a single 2D vortex. 3D motion is more evident at higher porous Rayleigh numbers and lower Darcy numbers.

Acknowledgments

One of the authors (J. Kramer) acknowledges the financial support of the research project Z2-2035, as provided by the Slovenian Research Agency ARRS.

References

[1] Beckermann C, Viskanta R, Ramadhyani S. A numerical study of non-Darcian natural convection in a vertical enclosure filled with a porous medium. Numerical Heat Transfer 1986;10:557–70.
[2] Lauriat G, Prasad V. Natural convection in a vertical porous cavity: a numerical study for Brinkman-extended Darcy formulation. Journal of Heat Transfer 1987;109:688–96.
[3] Lauriat G, Prasad V. Non-Darcian effects on natural convection in a vertical porous enclosure. International Journal of Heat and Mass Transfer 1989;32: 2135–48.
[4] Jecl R, Škerget L, Petrešin E. Boundary domain integral method for transport phenomena in porous media. International Journal for Numerical Methods in Fluids 2001;35:39.54.
[5] Baytas AC, Pop I. Free convection in a square porous cavity using a thermal nonequilibrium model. International Journal of Thermal Sciences 2002;41: 861–70.
[6] Basak T, Roy S, Paul T, Pop I. Natural convection in a square cavity filled with a porous medium: effects of various thermal boundary conditions. International Journal of Heat and Mass Transfer 2006;49:1430–41.
[7] Prasad V, Kulacki FA. Natural convection in horizontal porous layers with localized heating from below. Journal of Heat Transfer 1987;109:795–8.
[8] Kladias N, Prasad V. Natural convection in horizontal porous layers: effects of Darcy and Prandtl numbers. Journal of Heat Transfer 1989;111:926–35.
[9] Kladias N, Prasad V. Flow transitions in buoyancy-induced non-Darcy convection in a porous medium heated from below. Journal of Heat Transfer 1990;112:675–84.
[10] Storesletten L. Natural convection in a horizontal porous layer with anisotropic thermal diffusivity. Transport in Porous Media 1993;12:19–29.
[11] Dawood AS, Burns PJ. Steady three-dimensional convective heat transfer in a porous box via multigrid. Numerical Heat Transfer, Part A 1992;22:167–98.
[12] Sharma RV, Sharma RP. Non-Darcy effects on three-dimensional natural convection in a porous box. In: Annals of the assembly for international heat transfer conference, vol. 13; 2006. p. NCV-10.
[13] Wang QW, Zeng M, Huang ZP, Wang G, Ozoe H. Numerical investigation of natural convection in an inclined enclosure filled with porous medium under magnetic field. International Journal of Heat and Mass Transfer 2007;50: 3684–9.
[14] Wang QW, Yang J, Zeng M, Wang G. Three-dimensional numerical study of natural convection in an inclined porous cavity with time sinusoidal oscillating boundary conditions. International Journal of Heat and Fluid Flow 2010;31:70–82.
[15] Beck JL. Convection in a box of porous material saturated with fluid. The Physics of Fluids 1972;15:1377–83.
[16] Holst PH, Aziz K. Transient three-dimensional natural convection in confined porous media. International Journal of Heat and Mass Transfer 1972;15: 73–90.
[17] Zebib A, Kassoy DR. Onset of natural convection in a box of water-saturated porous media with large temperature variation. The Physics of Fluids 1977;20:4–9.
[18] Zebib A, Kassoy DR. Three-dimensional natural convection motion in a confined porous medium. Physics of Fluids 1978;21:1–3.
[19] Straus JM, Schubert G. Three-dimensional convection in a cubic box of fluid-saturated porous material. Journal of Fluid Mechanics 1979;91:155–65.
[20] Schubert G, Straus JM. Three-dimensional and multicellular steady and unsteady convection in fluid-saturated porous media at high Rayleigh numbers. Journal of Fluid Dynamics 1979;94:25–38.
[21] Horne RN. Three-dimensional natural convection in a confined porous medium heated from below. Journal of Fluid Dynamics 1979;92:751–66.
[22] Kimura S, Schubert G, Straus JM. Time-dependent convection in a fluid-saturated porous cube heated from below. Journal of Fluid Mechanics 1989;207:153–89.
[23] Stamps DW, Arpaci VS, Clark JA. Unsteady three-dimensional natural convection in a fluid-saturated porous medium. Journal of Fluid Mechanics 1990;213:377–96.
[24] Neto HL, Quaresma JNN, Cotta RM. Natural convection in three-dimensional porous cavities: integral transform method. International Journal of Heat and Mass Transfer 2002;45:3013–32.
[25] Neto HL, Quaresma JNN, Cotta RM. Integral transform solution for natural convection in three-dimensional porous cavities: aspect ratio effects. International Journal of Heat and Mass Transfer 2006;49:4687–95.
[26] Sezai I. Flow patterns in a fluid-saturated porous cube heated from below. Journal of Fluid Mechanics 2005;523:393–410.
[27] Ravnik J, Škerget L, Žunič Z. Velocity–vorticity formulation for 3D natural convection in an inclined enclosure by BEM. International Journal of Heat and Mass Transfer 2008;51:4517–27.
[28] Ravnik J, Škerget L, Hriberšek M. Analysis of three-dimensional natural convection of nanofluids by BEM. Engineering Analysis with Boundary Elements 2010, doi:10.1016/j.enganabound.2010.06.019.
[29] Popov V, Power H, Škerget L. Domain decomposition techniques for boundary elements application to fluid flow. Southampton, Boston: WIT Press; 2007.
[30] Bear J. Dynamics of fluids in porous media. New York: Dover Publications, Inc.; 1972.
[31] Nield DA, Bejan A. Convection in porous media. 3rd ed., Springer; 2006.
[32] Bear J, Bachmat Y. Introduction to modeling of transport phenomena in porous media. Kluwer Academic Publishers; 1991.
[33] Škerget L, Hriberšek M, Kuhn G. Computational fluid dynamics by boundary-domain integral method. International Journal for Numerical Methods in Engineering 1999;46:1291–311.
[34] Škerget L, Hriberšek M, Žunič Z. Natural convection flows in complex cavities by BEM. International Journal of Numerical Methods for Heat & Fluid Flows 2003;13:720–35.
[35] Wrobel LC. The boundary element method. John Wiley & Sons, LTD; 2002.
[36] Jecl R, Škerget L. Boundary element method for natural convection in non-Newtonian fluid saturated square porous cavity. Engineering Analysis with Boundary Elements 2003;27:963–75.